Astron. Astrophys. 110, 169–178

ASTRONOMY AND ASTROPHYSICS

Multifrequency High Resolution Observations of the Large Radio Galaxy B2 1321+31

R. Fanti[1], C. Lari[1], P. Parma[1], A. H. Bridle[2,3], R. D. Ekers[3], and E. B. Fomalont[4]

[1] Istituto di Fisica e Istituto di Radioastronomia, Via Irnerio 46, I-40126 Bologna, Italy
[2] Department of Physics, Queen's University at Kingston, Ontario K7L 3N6, Canada
[3] National Radio Astronomy Observatory P.O. Box O, Socorro, NM 87801, USA
[4] National Radio Astronomy Observatory, Edgemont Road, Charlottesville, VA 22901, USA

Received December 14, 1981; accepted March 15, 1982

Summary.

Observations at 49, 21 and 6 cm of the total and polarized intensity of the jets and extended lobes of the large radio galaxy B2 1321+31 are presented. The dominant component of the magnetic field in both jets is very regular and is oriented perpendicular to the jet axis. The degree of polarization increases with distance from the radio core, reaching values up to 40% and then decreases again to ∿ 20%. The depolarization ratio between 49 and 21 cm is about 0.8 in the inner parts of the jet and then increases outwards. The spectral index of the jets between 21 and 6 cm is unusually flat and constant, with $\alpha \sim 0.25$. The two jets expand initially at a constant angle ∿ 20° up to a distance from the core of ∿ 2' and then progressively stabilize to a transverse size of ∿ 45". The brightness in the jets does not everywhere follow the expectations based on a simple adiabatic expansion. A number of alternative explanations for this are considered. This effect and the dependence of depolarization on transverse size of the jet could both be explained if the flow velocity and/or mass flow increased with distance from the galaxy. Constraints on the expansion rate of the jets and on the energetics of the extended components suggest that the flow velocity in the jets is less than, or of the order of, several thousand km s^{-1}.

Key words : radio galaxies - jets in radio sources -

1. Introduction

The radio galaxy B2 1321+31 (NGC 5127) has been studied as a part of a systematic program of identification of radio sources of the Bologna second catalogue (B2) with galaxies of the "Catalogue of Galaxies and Clusters" (Colla et al. 1975). Subsequent observations with the Westerbork Synthesis Radio Telescope (WSRT) at 1.4 GHz (Ekers et al. 1981) showed that the radio source has a large angular size (∿ 12') and is strongly polarized. Its general appearence is of a bright, large and linear ridge of emission with faint wings, suggestive of a low brightness broad double source, superimposed on a very bright long twin jet.

The source, owing to its large angular size, is well suited for further observations at other frequencies with the WSRT, and we mapped it at 0.6 and 5.0 GHz. We also present VLA maps made at 1.4 GHz. The relevant parameters of the radio galaxy are summarized in Table 1.

The Hubble parameter is taken as H_o = 100 km s^{-1} Mpc^{-1}.

Table 1. Integral properties of B2 1321+31

Distance (Mpc)	48
m_{pg}	13.9
M_{pg}	-19.6
Total flux density at 0.6 GHz (Jy)[1]	2.9 ± .1
" " " " 1.4 "	1.75 ± .1
" " " " 5.0 "	0.6 ± .07
Spectral index[2]	0.65 ± .05
Optical position, RA	$13^h21^m26.3$
" " , dec.	31°49'33"
Total radio luminosity at 1.4 GHz (W Hz^{-1})	4.8 10^{23}
Angular size (arcsec)	700 x 200
Linear size (Kpc)	160 x 46

1) 1 Jy = 10^{-26} W Hz^{-1} m^{-2}
2) $S(\nu) \propto \nu^{-\alpha}$

2. The observations and data reduction.

The radio brightness distribution of the source has been mapped at 0.6, 1.4 and 5.0 GHz, using the WSRT (Hogbom and Brouw, 1974). The relevant parameters of these observations are summarized in Table 2a. The standard reduction procedures (van Someren Greve, 1974) were followed and maps in all Stokes parameters were obtained at the three frequencies. The maps were cleaned and restored using the CLEAN algorithm developed by Hogbom (1974).

In order to compare the data at different frequencies we also produced convolved 5 GHz maps with the same resolution as those at 1.4 GHz and convolved 1.4 GHz maps with the resolution of those at 0.6 GHz. These maps are referred to as low resolution maps at 5.0 and 1.4 GHz. Details of these maps are given in Table 3a. The maps at different frequencies which are used for comparison were restored using identical gaussian beams.

In producing the maps to be compared at the various frequencies, we tried to match the baseline coverages as much as possible. This generally required omission of the longest baselines in the higher frequency maps (leaving only ≃ 30% of the original coverage) and of a few (1 - 2) short baselines in the lower frequency map. The main difference in the remaining baseline coverage is at the shortest spacings. Here the missing baselines introduce depressions in the zero level, which, in general, vary across the maps. Since the minimum baselines at the two frequencies cannot be exactly the same, the zero offsets are different and this is responsible for systematic

Send offprint requests to: R. Fanti

TABLE 2a. OBSERVATIONAL PARAMETERS FOR WSRT

Frequency (GHz)	0.6	1.4	5.0
Obs. Date	October 78	October 74	May 79
Obs. Time (hours)	12	12	12
Interferometer Spacing (m.)	54 + *n* 72 234 + *n* 72	72 + *n* 72	54 + *n* 72 234 + *n* 72
Radius 1st Grating	46' x 89!2	10' x 19'	6' x 11.6'
Primary Beam	84'	34'	10'
Number of Interferometers	40	20	40

TABLE 2b. OBSERVATIONAL PARAMETERS FOR VLA

Obs. date	September '79
Obs. time	10^h
Minimum spacing	70 m
Maximum spacing	21000 m
Primary beam	9!0
No. of interf.	120

TABLE 3a. WSRT MAP PARAMETERS

Frequency (GHz)	Half power beamwidth (arcsec)	Interferometer spacings shortest/increment/longest (wavelengths)	R.M.S Noise at field center (mJy/beam)	Off-set zero leve mJy/beam
5.0	6 x 12	900/ 600 /26690	0.4	-
5.0	24 x 45.5	900/ 600 /6898	0.7	-3
1.4	24 x 45.5	1019/ 343 /6796	1.0	-2
1.4	24 x 45.5	343/ 343 /6796	1.0	-3
1.4	49 x 93	343/ 343 /3398	1.6	-3
0.6	49 x 93	402/ 73.5/3252	1.8	-2.5
0.6	49 x 93	256/ 73.5/3252	1.8	-2.0

TABLE 3b. VLA MAP PARAMETERS

1.4	2" x 3"	20 km. taper	0.15
	6" x 12"	5 km. taper	0.30

errors in any comparison. Furthermore,the depression would be different even for equal baseline coverages if the source structure changed with frequency. The use of the CLEAN algorithm corrects for the above problems to some extent,but it is difficult to asses the accuracy of this quantitatively. Errors will be discussed in the next sections,case by case (in every comparison).

For unknown reasons the 5 GHz observations were made with a pointing position displaced from the center of the source by about 2!5 to the NW,roughly at the center of the NW broad component. The off-set pointing position, combined with the small primary beam of the WSRT,introduces an attenuation across the source which is not symmetric with respect to the center. The map has been corrected for this attenuation effect. However,the errors are not symmetric with respect to the center and are particularly large in the farthest half of the SE jet. This,for instance,strongly limits the use of the 5 GHz map in the determination of the spectral index across the source,which can be determined with good accuracy only in the NW jet.

The source was observed also at the VLA at 1.4 GHz. The relevant parameters of the observations are given in Table 2b. The characteristics of the VLA maps are summarized in Table 3b. The reduction procedure is similar to the one used for the WSRT observations.

Figs. 1 to 5 show the VLA and WSRT maps of the source at the various frequencies. The source morphology can be best described as the superimposition of a long bright symmetrical two-sided jet,easily visible in the VLA and WSRT 5.0 and 1.4 GHz maps,on a double source with broad components of sizes $\simeq$ 4-5 arcmin,best seen in the 0.6 GHz WSRT map. A weak nucleus can be seen in the higher resolution maps.

Integrated flux densities are given in table 1. The value obtained from the 5 GHz map is an underestimate of the true source flux,since the source is largely resolved at even the shortest spacing ($\sim$ 900 wavelengths). It is largely contributed by the jet flux.

The various components of the source are discussed in the next sections.

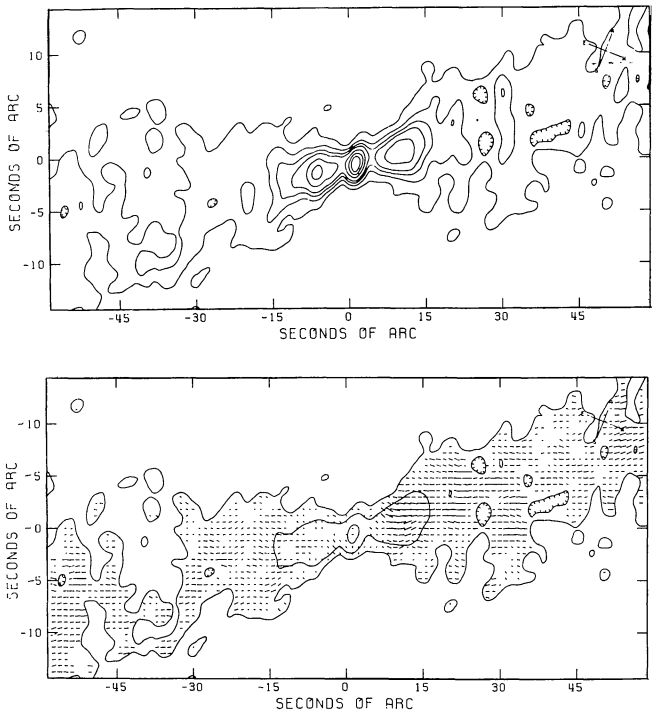

Fig. 1. VLA maps at 1.4 GHz,with a resolution of 2"x3" (beam major axis is at -30°). The ellipse at the upper left shows the beam FWHM. Top: total intensity map;contours are .6,1.2,1.8,2.4,3.6,4.8,6.0 mJy/beam. Bottom: electric vector polarization map,superimposed on some total intensity contours.

3. The nucleus.

The core is best seen in the high resolution VLA map (Fig. 1),where it is well resolved from the jet. The compar son of the VLA 1.4 GHz and the WSRT 5.0 GHz maps with the same resolution shows that the core has an inverted spectrum between those two frequencies. The parameters of the core are summarized in Table 4.

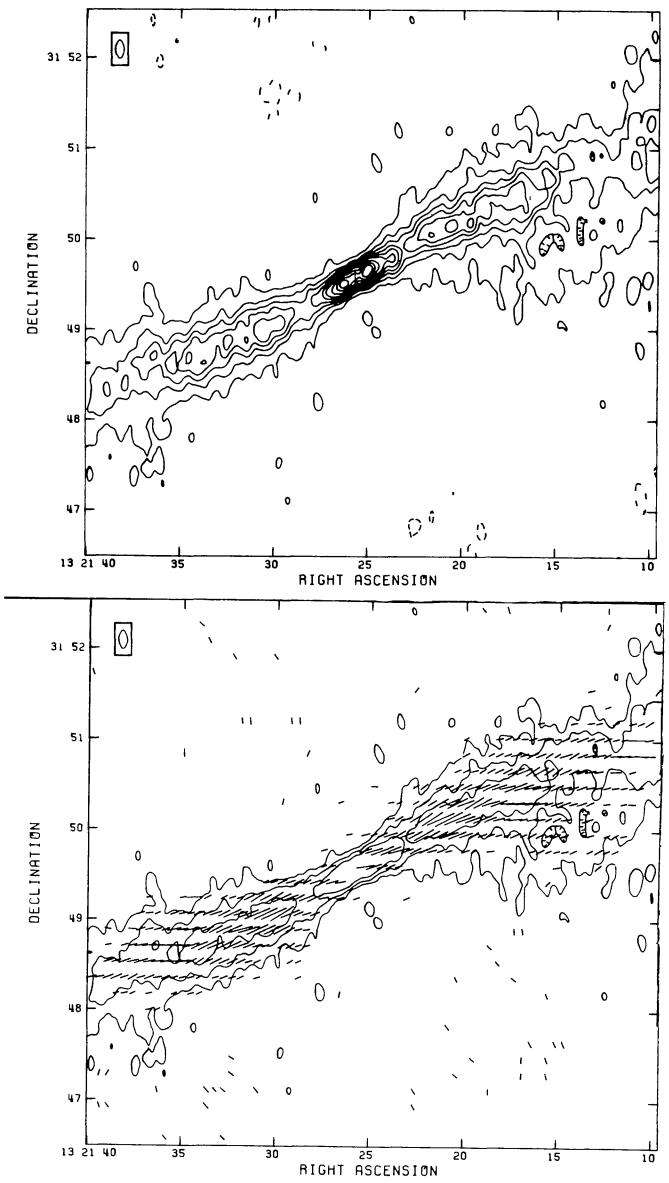

Fig.2 VLA maps at 1.4 GHz,with resolution of 6"x12" (p.a. of major axis is 0°). The ellipse at the upper left shows the beam FWHM. Top: total intensity map;contours are : -1(dashed),1,2,3,4,5,6,8,10,12 mJy/beam. Bottom: electric vector polarization map,superimposed on some total intensity contours.

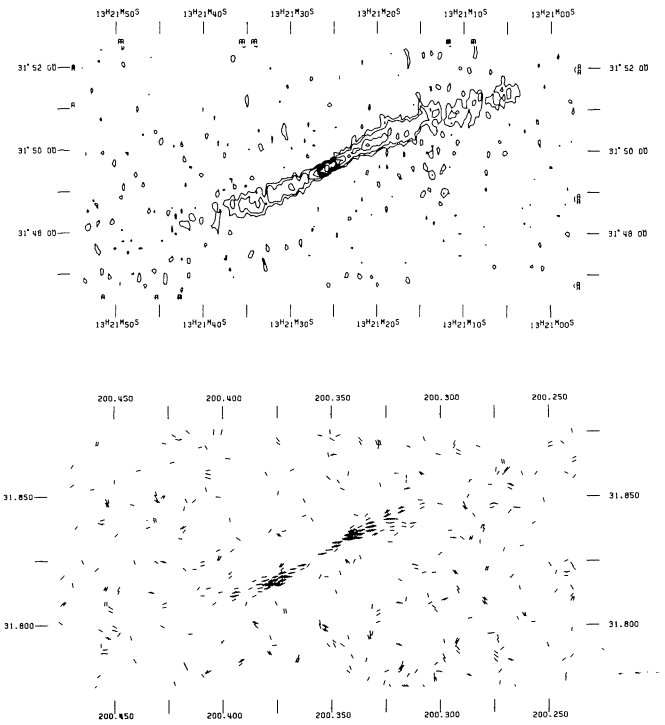

Fig. 3. WSRT maps at 5.0 GHz. The resolution is 6"x12". Top: total intensity map;contours are: 0.5,1.,2.,3.,4., 5.,10. mJy/beam. Bottom: electric vector polarization map.

Table 4. Core Parameters

Right Ascension	$13^h21^m25^s.78$
Declination	31°49'33".4
Flux density at 1.4 GHz (VLA)	7.7 mJy
Flux density at 5.0 GHz (WSRT)	21.0 "
Spectral index	-0.8
Angular size	<0".5
Radio Luminosity at 1.4 GHz	$2\ 10^{21}$ W Hz^{-1}
% pol. / p.a. / ν	∿5% / -10° / 1.4 GHz <6% / / 5.0 "

4. The two jets

a) The structure

The jets are easily visible in all maps presented,including the low resolution 0.6 GHz map,on which they appear as a bright ridge of radiation superimposed on the double structure.

The jets are oriented along p.a. ≃ 115°,about 30° from the minor axis of the galaxy (Battistini et al. 1980).

The VLA higher resolution map displays the structure of the inner regions of the jets. The jets are very symmetric and both sides brighten rapidly at ∿ 5" (∿1 kpc) from the core,which appears as a very distinct entity. On both sides of the core,the bright regions at the base of the jets extend for about 10" along the main radio axis.

The brightness along the jets shows several enhancements and depressions which are easily seen in both the VLA and WSRT maps at equal resolution.The NW jet seems to be longer,extending over ∿5',as compared to the ∿3' extension of the SE one. The brightness decreases slowly outwards and no bright spots are seen at the ends. The bright condensations seen at the ends in the 1.4 GHz map have no counterparts in the higher resolution maps and are likely to be effects of beam integration over slowly modulated brightness changes.

At about 2 - 3 arcmin (30 - 40 kpc) from the core, the jets bend on both sides with an S type (or inversion) symmetry. The amplitude of the bending is ∿ 10°.

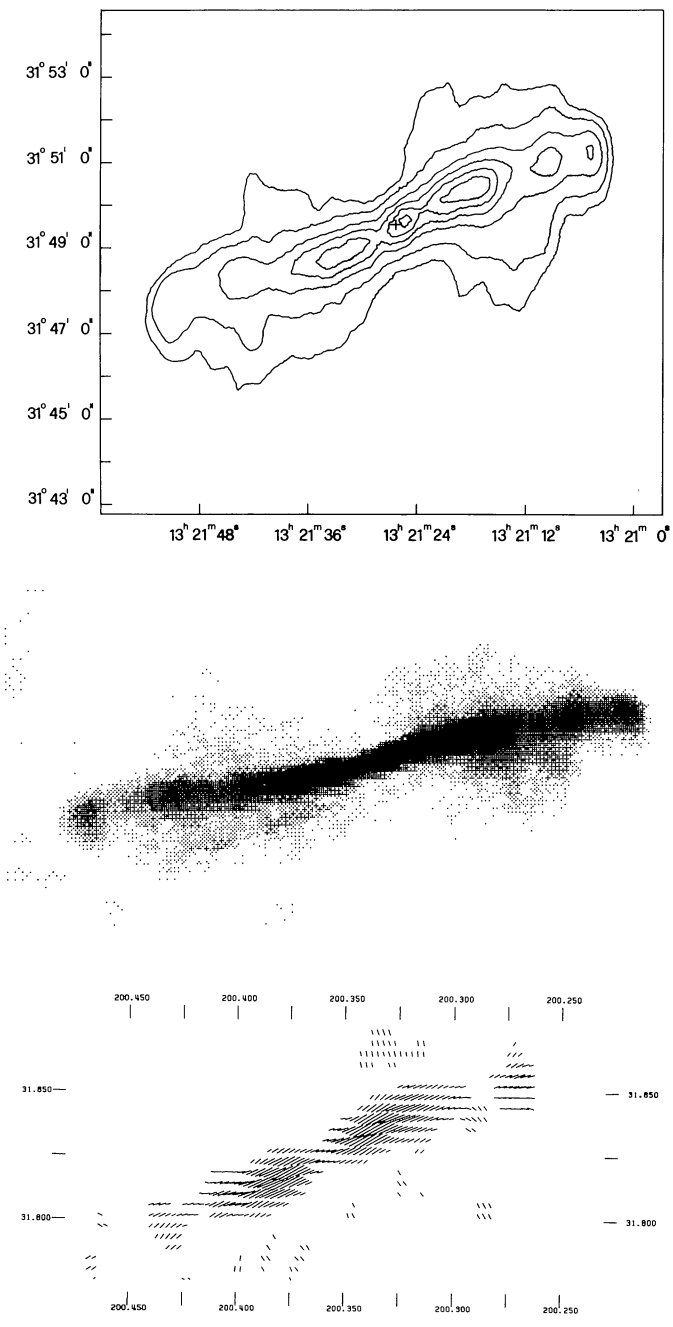

Fig. 4. WSRT maps at 1.4 GHz. The resolution is 24"x45". Top: total intensity map; contours are : 5, 10, 20, 30, 40, 50 mJy/beam. Center: radio photo of total intensity map;the declination scale is compressed by a factor $(\sin \delta)^{-1}$. Bottom: electric vector polarization map.

We have measured the half-intensity widths of the jets as a function of the angular distance from the radio core,by making cross cuts along the full resolution 5 GHz WSRT map and the VLA map with the same resolution, in direction perpendicular to the jet orientation. The deconvolved half-widths are plotted in fig.6 as a function of the distance from the center. The transverse brightness profiles are center brightened and have been treated as gaussians in making this deconvolution.

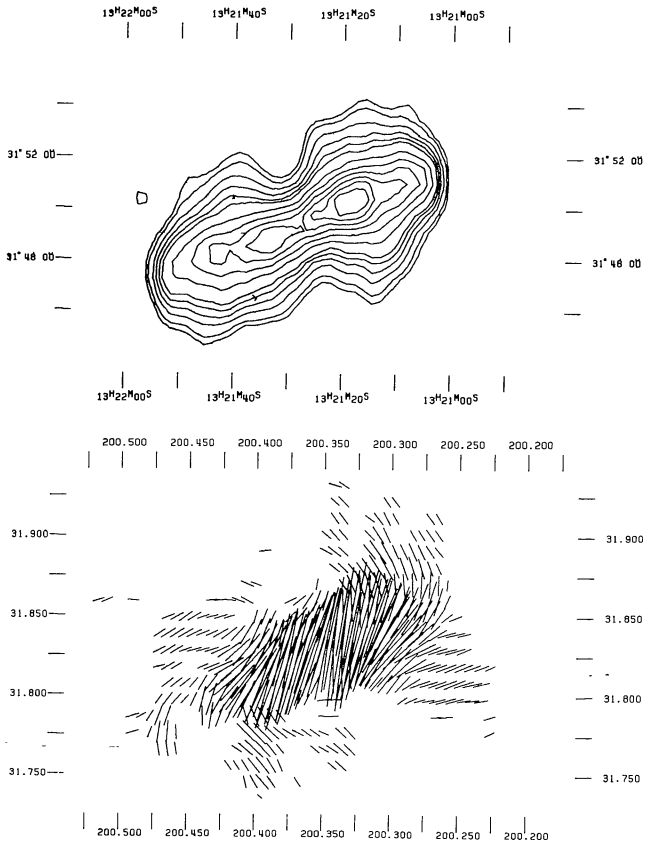

Fig. 5. WSRT maps at 0.6 GHz. The resolution is 49"x93". Top : total intensity map; contours are 2.5,5.0,7.5, 10.0,20.,30.,40.,50.,75.,100.,125.,150. Bottom: electric vector polarization map.

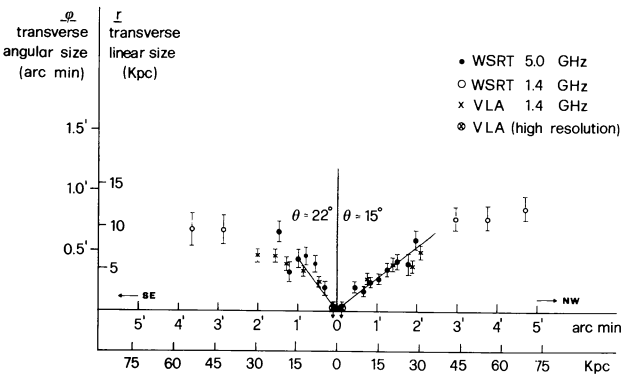

Fig. 6. Cross sectional widths (FWHM) for the jets as a function of distance from the central source. The full line is an eye fit to the data for the range of distances where the expansion is considered linear (see text).

Errors mostly derive from uncertainties in the zero level and may easily correlate from point to point. The study of the opening angle of the jets is limited,in the higher resolution maps,to the first $\pm$ 2' from the nucleus by the signal to noise ratio. In this range of distances from the center,the western jet has a constant half opening angle of 8° $\pm$ 2°. The eastern jet appears to open more rapidly with a half opening angle of 11°

± 3°. Further away from the core the jet width can be estimated better from the WSRT 1.4 GHz map. It seems that the jet opening angle decreases and that the transverse half-width of the jets stabilizes around a value of ∿ 45" ± 8" (10 ± 2 kpc).

The jets are strongly polarized at all frequencies. The polarized intensity is quite noisy in the WSRT 5.0 GHz full resolution map,but it is easily measurable in all the other maps. The fractional polarization at 1.4 GHz is shown in fig.7,as a function of distance from the center. The fractional polarization has a minimum (∿5%) in the inner regions of the jet (within ± 10",or ± 2 kpc,from the nucleus). At a distance of ∿ 30" (∿6kpc) from the nucleus the fractional polarization has increased to ∿ 40% or more,and then,at distances larger than 2' (28 kpc), it declines slowly while remaining generally at levels ≳ 20%. The fractional polarization is similar at 5.0 and 1.4 GHz,but is somewhat lower at 0.6 GHz.

Fig.8 shows the position angle of the electric vector at various frequencies. The orientation of the vector is very uniform along the jet: local variations are generally ≲ 10°. Its orientation,at 1.4 and 5.0 GHz,correspond to the orientation of the jet,except in the innermost regions (± 10") where,however,the errors are larger. At 0.6 GHz the electric vector is rotated,with respect to the higher frequencies,by 40°-50°.

The integrated parameters of the jets are given in table 5.

Table 5. Parameters of the jets.

Frequency (GHz)	5.0	1.4	0.6
Flux density (mJy)	550±70	800±100	
Fractional polarization	20 %	21 %	16 %
Position angle of polarization	110°	112°	155°
Spectral index	0.3 ± 0.14		
Radio Luminosity at 1.4 GHz (W Hz^{-1})	$2.2\ 10^{23}$		
Maximum length (kpc)	2 x 80		

b) The spectral index distribution along the jets.

We have used the WSRT maps at the various frequencies to derive two frequency spectral index distributions, in various locations, along the jets. In doing this attention has been paid to comparing maps made with similar resolution and with spatial frquency coverages that are as similar as possible (see also section 2). The results of the comparison are shown in fig.9. Since all the maps at the three frequencies have average negative off-sets of ∿ 2-3 mJy/beam,corrections have been applied for this effect. The quoted errors include an allowance for uncertainties in the zero level.[1]

The spectrum of the jet in the high frequency range (1.4 - 5.0 GHz) is remarkably flat (α ∿ 0.3),flatter than that in any other presently known radio jet. Within the errors it is also constant all over the jet.

[1] It is stressed that the maps used for the 5.0/1.4 GHz comparison have been computed using only interferometers with spacings larger than ∿ 900 wavelengths. The broad components are then completely filtered out and the spectral index distribution obtained refers only to the jet.

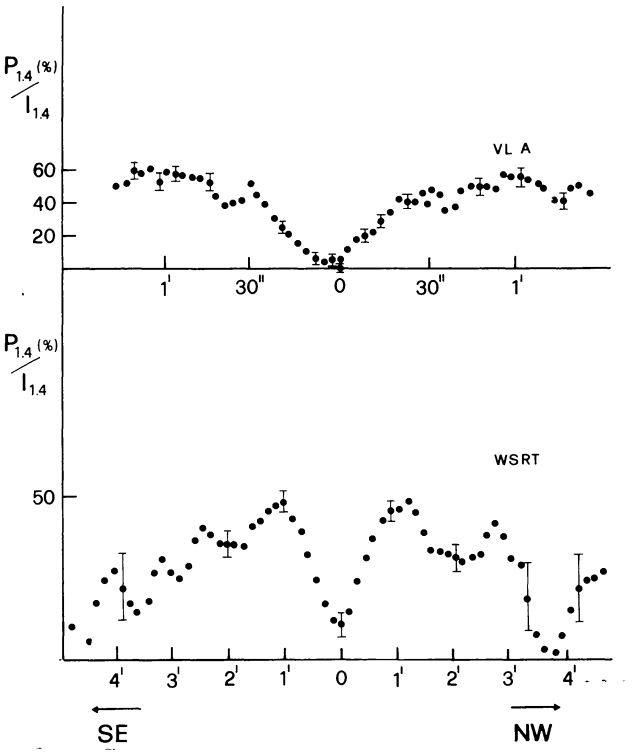

Fig. 7. Plot of the percentage polarization at 1.4 GHz along the jets. Top: from the VLA map (resolution 6"x10"). Bottom: from the WSRT map.

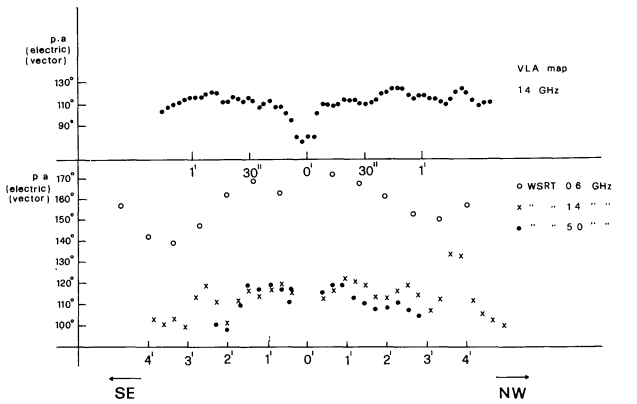

Fig. 8. Plot of the position angle of the electric vector of the polarized radiation,along the jets. Top: VLA map (resolution 6"x12"). Bottom: WSRT maps at the three frequencies.

Within ± 1.5' (20 kpc) from the core,we have also derived the high frequency spectral index by comparing the VLA 1.4 GHz map and the WSRT 5.0 GHz map with equal resolution. This spectral index distribution is displayed in fig. 9 . There is a systematic difference from the spectral distribution shown in fig.9a,by Δα ∿ 0.2. This is likely to be due to the presence,in the VLA map,of the broad components,which completely surround the jet and produce an off-set ≳ 1 mJy/beam. The broad components are absent in the 5.0 GHz WSRT map (see section 2).The off-set in the VLA map,due to the presence of the broad components allows for an increase of the spectral index

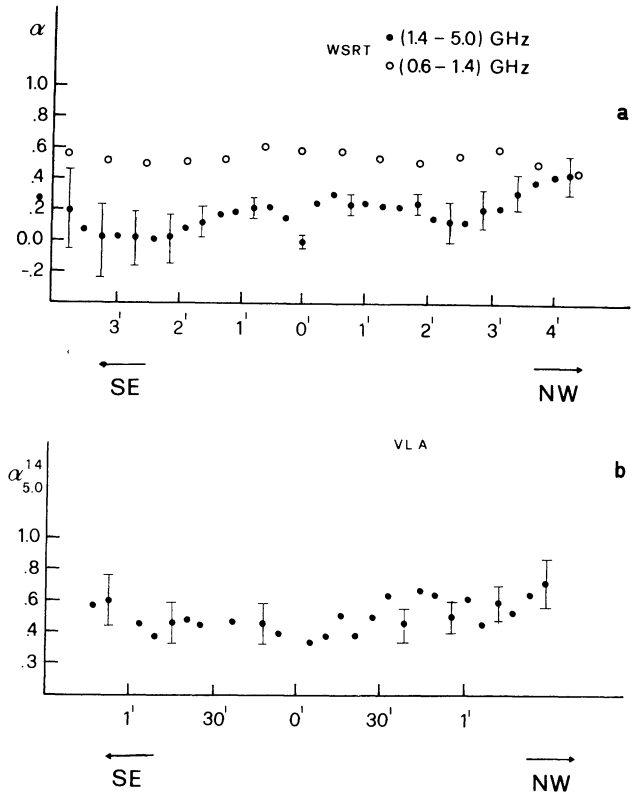

Fig. 9. Plot of the spectral index along the jets. Top: $\alpha^{5.0}_{1.4}$ and $\alpha^{1.4}_{0.6}$ from comparison of WSRT maps with equal resolution. Bottom: $\alpha^{5.0}_{1.4}$ from comparison of the WSRT 5.0 GHz and VLA 1.4 GHz maps with resolution of 6" 12".

$\Delta\alpha \gtrsim 0.15$, which is enough to remove most of the difference in the two determinations of the spectral index. In the lower frequency range (0.6 – 1.4 GHz) the spectrum appears considerably steeper and again constant along the jet. However we note that in this frequency range we have a considerable contribution from the broad components and the observed radio spectrum is an average of the spectrum of the jet and that of the broad components.

c) Minimum energy parameters in the jets.

We have computed the equipartition magnetic field and energy density in the jets, using standard formulae (Pacholczyk 1970) and a ratio of proton to electron energies equal to unity. The radio spectrum is assumed to extend from 10 to 10^4 MHz. The assumed geometry is cylindrical with a filling factor equal to 1. Results for various locations along the jet are listed in table 6.

The values for the magnetic field and energy density are very similar to those found for NGC 315 (Willis et al. 1981). The computed magnetic field decreases along the jet. However this should be taken with caution, not only due to the uncertainties from the usual assumption which enter in the computations, but also because even if the assumption of equipartition holds in some part of the jets, it would not hold in other parts in case of two dimensional adiabatic expansion (see again Willis et al. 1981).

TABLE 6. PHYSICAL PARAMETERS FOR SOME LOCATIONS ALONG THE JET

Distance from core		$b_{1.4}$	Transverse size		Dep. 50/21	H_{eq}	u_{min}	$n_e\ 10^4$
arcmin	Kpc	mJy/arcsec^2	arcsec	Kpc		μG	erg/cm^3	cm^{-3}
4.0	57.6	$2.0\ 10^{-2}$	(45.0)	10.8	≥ 0.90	2.9	$6.9\ 10^{-13}$	< 2.5
3.0	43.0	$1.4\ 10^{-2}$	(45.0)	10.8	0.90	2.7	$5.7\ 10^{-13}$	$2.7\ ^{+0.9}_{-1.2}$
2.0	28.8	$6.0\ 10^{-2}$	30.0	7.2	0.80	4.5	$1.6\ 10^{-12}$	3.6 ± 0.7
1.0 NW	14.0	$8.0\ 10^{-2}$	15.5	3.8	0.80	5.9	$2.8\ 10^{-12}$	5.2 ± 1.0
0.5	7.2	$1.2\ 10^{-1}$	8.0	1.9		8.0	$5.2\ 10^{-12}$	
0.5	7.2	$1.1\ 10^{-1}$	5.5	2.3		7.5	$4.4\ 10^{-12}$	
1.0 SE	14.0	$7.5\ 10^{-2}$	20.0	4.8	0.85	5.4	$2.3\ 10^{-12}$	3.8 ± 1.3
2.0	28.8	$4.0\ 10^{-2}$	(35.0)	8.4	0.78	3.9	$1.2\ 10^{-12}$	3.4 ± 0.8
3.0	43.0	$1.4\ 10^{-2}$	(40.0)	8.4	1.00	2.8	$6.0\ 10^{-13}$	< 2.5
4.0	57.6	$1.5\ 10^{-2}$	(40.0)	8.4	1.00	2.8	$6.3\ 10^{-13}$	"

d) The foreground rotation measure and the orientation of the magnetic field.

The position angle of the electric vector at the various frequencies is remarkably constant all over the source, as already noted. Moreover no significant change is seen between 5.0 and 1.4 GHz. A measure of the integrated position angle at 2.7 GHz (Parma and Weiler 1981) is again consistent with the values at the two other frequencies. At 0.6 GHz the position angle is rotated by 40° – 50°. From these data we can determine the rotation measure without any ambiguity. The rotation measure is

$$RM \sim 3 - 4.5 \text{ rad/m}^2$$

Such a small value of RM is consistent with an origin in the foreground Faraday screen of our galaxy. The average rotation measure of nearby radio sources, derived from Tabara and Inoue (1980), is -2 rad/m^2 ($\sigma \sim 7$ rad/m^2).

The small value of the RM implies that the intrinsic E-vector position angle is within a few degrees of that at 5.0 GHz. The projected magnetic field is therefore oriented at $\sim 25°$, almost exactly perpendicular to the jet axis, except within about 10" (2 kpc) of the nucleus where it may be at an angle of $\sim -10°$. This is similar to the configuration found in other jets of low luminosity sources such as 3C31, NGC 315 (Fomalont et al.1980) and 3C 449 (Perley et al.1979).

We note that at 0.6 GHz, where we see a large rotation from the intrinsic position angle, the position angle changes regularly from the inner regions of the jets and then goes back to the original value in the outer edges. The maximum change occurs $\simeq$ 3'-4' from the nucleus, in positions which roughly correspond to the central regions of the two broad components. It is tempting to interpret these differential variations as due to the Faraday rotation of the polarized radiation of the jets in the broad components. We therefore assume an almost constant major contribution to the rotation measure of ~ 4 rad/m^2, presumably due to our galaxy, and a modulation with maximum amplitude ~ 1 rad/m^2 as due to the broad components.

e) The depolarization along the jets.

A comparison of the polarized intensity distribution at the frequencies of 1.4 GHz and 0.6 GHz (after convolution to equal resolution) is shown, in fig.10, as depolarization ratios along the jets.[2] Corrections have

[2] The depolarization ratio is defined as the ratio between the fractional polarization at 0.6 GHz to that at 1.4 GHz.

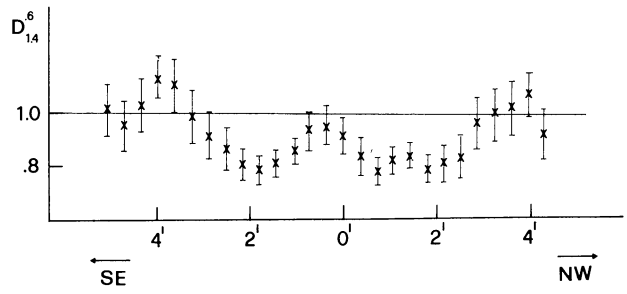

Fig. 10. Plot of the depolarization ratio $D^{0.6}_{1.4}$ between 0.6 GHz and 1.4 GHz, along the axis of the jets.

been applied for the zero level off-sets present in the maps. Errors account for noise and uncertainties in the off-set levels. The jets, which are not depolarized between 1.4 and 5.0 GHz, are significantly depolarized between 1.4 and 0.6 GHz. The average depolarization ratio between the two latter frequencies is $\simeq 0.9 \pm 0.05$. It is ~ 0.8 in the inner regions and increases outwards.

f) Intrinsic degree of polarization and ratio of ordered to random magnetic field.

The intrinsic degree of polarization is related to the ratio between the ordered component of the magnetic field H_o and the random component H_r (Burn 1966) :

$$P_i = P(\alpha) \frac{H_o^2}{H_o^2 + H_r^2} = \frac{3\alpha + 3}{3\alpha + 7} \frac{H_o^2}{H_t^2}$$

where α is the spectral index, H_t the total magnetic field and $P(\alpha)$ the degree of polarization for a perfectly ordered field.

Since no depolarization is seen between 5.0 and 1.4 GHz and little at 0.6 GHz, we take the fractional polarization at 1.4 GHz as representative of the intrinsic degree of polarization (we prefer to use the measurement at 1.4 GHz, because of its better signal to noise ratio).

The degree of polarization shows a regular change along the jet (fig.7) going from 40% - 50% in the range of distances 30" - 2' from the core down to $\sim$ 20% in the outer parts of the jet. This implies :

$H_o/H_r \sim 1.5$ 30" < distance < 2'

" ~ 0.7 " > 3'

The field is therefore very regular, with the exclusion of the first $\pm$ 30", but progressively becomes more irregular as one proceeds toward the outer parts.

g) Thermal particle density in the jets

One of the most striking characteristics in B2 1321+31 is the very low and slowly changing depolarization ratio between 0.6 and 1.4 GHz. Assuming that this depolarization is due to differential Faraday rotation, describing the jet in terms of the "slab model" (Burn 1966) and neglecting the effect of the disordered component of the magnetic field, we deduce :

$$(RM)_i = 2.6\ 10^{-17}\ H_{oz}\ n_i\ r \sim 1 - 4\ rad/m^2$$

H_{oz}, n_i and r are the component of the ordered magnetic field along the line of sight, the internal density of thermal electrons and the transverse width of the jet and $(RM)_i$ is the internal Faraday rotation measure.

Assuming the component of the ordered magnetic field along the line of sight to be

$$H_{oz} \sim 0.5\ H_{eq}$$

and assuming as transverse size of the jet at the various positions that deduced from figure 6, we obtain thermal plasma densities in the range of $10^{-3} - 10^{-4}$ cm^{-3}. Similar values have been deduced for the jet in NGC 315 (Willis et al. 1981).

An alternative explanation for the depolarization seen between 1.4 and 0.6 GHz is possible however, namely that at the lower frequency we are seeing a superimposition of the jets on the more prominent broad components. If they are less polarized than the jets, a decrease of the total degree of polarization could result from superposition effects alone. Such a superposition might also explain the regular change of the position angle of the electric vector at 0.6 GHz along the jets. The expected amount of depolarization resulting from superimposition alone, although quite difficult to be determined owing to uncertainties on the relevant parameters of the broad components, is probably < 10%. Furthermore its maximum value is expected to occur close to the centers of the broad components, namely $\sim$ 3'-4' from the core, while the observed depolarization is maximum at distances $\lesssim$ 2', where the effects of superimposition should be marginal.

We therefore consider below the consequences of interpreting the observed depolarization as being due to internal Faraday rotation.

5. The broad components

The source exhibits, in the 0.6 GHz WSRT map, a clear double structure. The jets, however, are still very bright and this makes it difficult to determine the structure and properties of the two broad components.

They are $\sim$ 3' - 4' in diameter (40 - 50 kpc) and have a separation of similar amount.

By subtracting the jet fluxes to the integrated fluxes one gets an estimate of their integrated spectra, which seem rather steep ($\alpha \sim 1.0 \pm 0.2$). Clearly, further observations at 0.6 GHz with higher resolution are needed to improve the knowledge of the low frequency spectrum in the jets and in the broad components.

Polarization is also seen in the broad components, outside the main jets, with rather large polarization fractions ($\sim$ 20 - 30 % at 1.4 GHz).

Table 7 gives the intrinsic parameters of the extended components of the source. Magnetic field and energetics are computed on the basis of the equipartition assumptions. The density of the thermal plasma is derived assuming that the modulation seen in the position angle of the electric vector along the jet, at 0.6 GHz, is due to Faraday rotation in the broad components. The temperature is deduced assuming that the thermal plasma confines the jet at distances larger than $\sim$ 3' (see section 6c). For comparison we give the parameters of the radio galaxy B2 0924+30, a wide double source studied by Ekers et al. (1981), which is similar to B2 1321+31 in size and luminosity but has no jets.

It is worth noting again that the broad components completely surround the two jets, a situation rather unusual (but see also B2 0326+39, Bridle et al., in preparation), compared to other radio galaxies with jets. In particular, looking at fig.4, one is led to think that the broad components are built up by some kind of leakage all along the jets, rather than being fed by the heads as generally envisaged in the case of strong radio sources (e.g. Hargrave and McEllin 1975).

TABLE 7. INTRINSIC PROPERTIES OF THE BROAD COMPONENTS

	B2 1321+31	B2 0924+30
Radio Luminosity at 1.4 GHz (W Hz^{-1})	$1.3\ 10^{23}$	$1.7\ 10^{23}$
Component sizes (Kpc)	45	80
Volume (cm^3)	$1.5\ 10^{69}$	$7.0\ 10^{69}$
Equipartition energy density (erg/cm^3)	$2.0\ 10^{-13}$	$6.0\ 10^{-14}$
Minimum energy (ergs)	$3.0\ 10^{56}$	$4.0\ 10^{56}$
H_{eq} (gauss)	$1.4\ 10^{-6}$	$0.8\ 10^{-6}$
n_i (cm^{-3})	$4.0\ 10^{-5}$	
Thermal plasma mass ($M_\odot$)	10^8	
Temperature (°K)	$< 10^8$	
Thermal energy (ergs)	$< 2\ 10^{57}$	
Alfven velocity (km/sec)	$6\ 10^2$	

6. Discussion

In the following discussion we assume that the twin bright features emanating from the core, which we refer to as jets, do really represent a transport of energy and matter, at some speed v_{fl}, from the nucleus to the outer components. Furthermore we will use physical parameters derived from assumption of equipartition and given in table 6. That this assumption can be incorrect has been mentioned earlier and should be kept in mind by the reader in the next paragraphs.

a) Expansion of the jets; variations of surface brightness and plasma density along the jet. Is the flow velocity constant ?

As previously seen, the jets open at a roughly constant angle of $\sim 20°$ up to a distance of 1'- 2' from the core. As the jets expand we expect that the brightness $b_s(\nu)$ should decrease because of adiabatic energy losses of the relativistic electrons and decrease of the magnetic field due to flux conservation. Depending on whether or not the particles do work during the expansion we should have :

$$b_s(\nu) \propto r^{-(7/3)\alpha-2} \quad \text{or} \quad b_s(\nu) \propto r^{-2-\alpha}$$

For $\alpha \sim 0.3$ we obtain :

$$b_s(\nu) \propto r^{-2.7} \quad \text{or} \quad b_s(\nu) \propto r^{-2.3}$$

in the absence of field amplification or particle reacceleration.

In fig. 11 a,b we show the surface brightness of the jet at 1.4 GHz as a function of the jet angular FWHM ϕ. Also plotted (as a solid line) is the prediction, on the assumption of adiabatic expansion, with $b_s(\nu) \propto r^{-2.5}$, intermediate between the two extremes noted above. In the ranges $\phi < 10''$ and $\phi > 25''$ the brightness decreases about as fast as the prediction. However, for $10'' < \phi < 25''$ the brightness stays almost constant (or perhaps even increases).

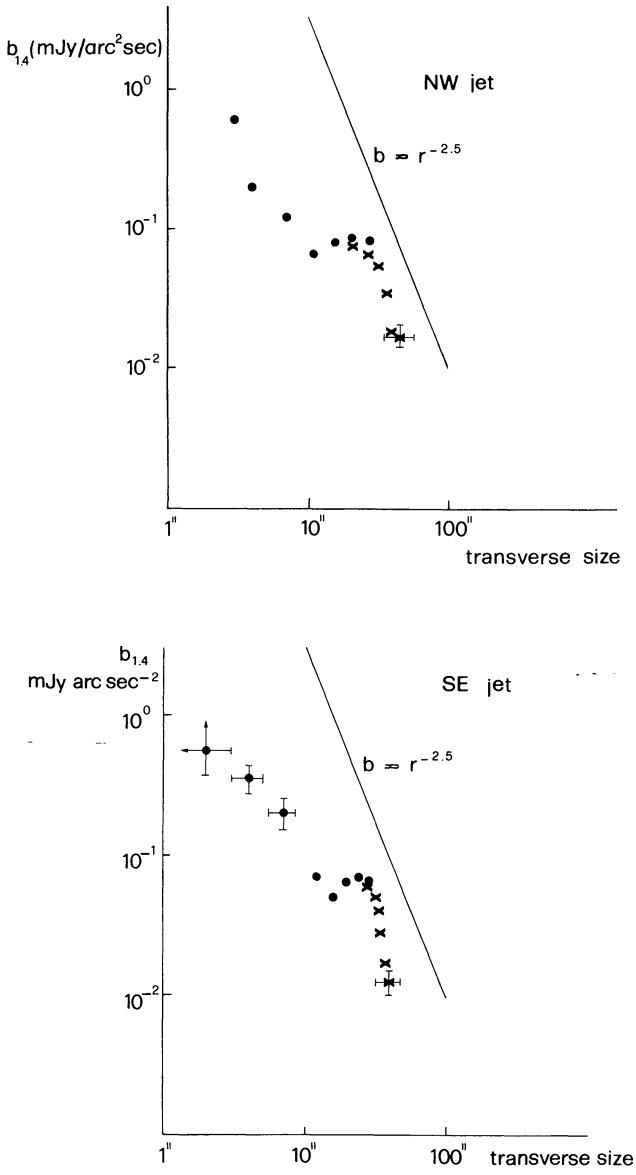

Fig. 11. Logarithmic plot of jet brightness (mJy/arcsec^2) as a function of transverse jet size.

A similar situation has been noted in several other jets. In particular see Willis et al. (1981) for NGC 315, where it is noted that the surface brightness drops off more rapidly as a function of the jet width in those regions where the rate of jet expansion is low and vice-versa.

The brightness behaviour can be explained if in situ relativistic particle acceleration and/or field amplification occur, possibly due to reconversion of turbulent energy carried in the flow (e.g. Henriksen et al. 1982).

An alternative possibility may be that the flow velocity decreases along the jet (e.g. due to entrainment of the surrounding material). This would be equivalent to a longitudinal compression of the system of particles and magnetic field, which can act to reduce the adiabatic losses. It is easy to see that, in this case, the dependence of brightness on velocity flow is described by the additional factor :

$$v_{fl}^{-(2+\frac{5}{3}\alpha)}$$

In order to obtain a plateau in brightness in the "constant region", we require:

$$v_{fl} \propto r^{-\beta} \qquad \beta \sim 0.8 - 1.0$$

This alternative possibility may be important if the jets do not carry other forms of energy (like kinetic energy, turbulent energy, etc...) suitable for reacceleration.

If we assume a constant mass flow along the jet, magnetic flux conservation and constant v_{fl}, we would expect:

$$(RM)_i \propto H_{oz}\, n_i\, r \propto r^{-2}$$

and this would imply a fast increase in the depolarization ratio in the "constant region" where the jets widen quickly. On the contrary the observed depolarization ratio is constant in that region. This is similar to what was found by Willis et al.(1981) in the case of NGC 315. The observed dependence of the depolarization ratio on r indicates:

$$H_{oz}\, n_i\, r \sim \text{constant}$$

If, in view of the constancy of $b_s(\nu)$, discussed above, we assume $H_{oz} \sim$ const. in the "constant region", then:

$$n_i \propto r^{-1}$$

This result may also be explained if there is a decrease in v_{fl} along the jets, due to loss of momentum at the boundaries of the jets and/or to entrainment of external matter. Assuming either conservation of the mass flow $\dot{M}$ (but not of momentum flow) or conservation of the momentum flow plus entrainment, we deduce

$$\beta \sim 1.0 \qquad \text{or} \qquad \beta \sim 0.5$$

respectively.

b) The flow velocity along the jets and the energetics

Methods used to estimate flow velocity in the jets are discussed by Willis (1981). One of the most commonly used is based on the assumption that the jets are "free". In this case the jets, assumed to be strongly supersonic, expand sideways, confined only by their own inertia, with a constant opening angle determined by the ratio of the expansion velocity v_{exp} ($\sim$ sound speed $\sim$ 700 km/sec) to the flow velocity. From the opening angle θ we deduce:

$$v_{fl} \sim (6 \pm 1)\, v_{exp} \sim 3500 - 4900 \text{ km/sec}$$

This method gives similar values when applied to other jets. It may be unreliable however, since it is not clear at all that the jets are "free". Considering the possibility of partial transversal confinement, the value of v_{fl} deduced from the "free jet" assumption has to be taken as an upper limit.

If we express the velocity flow in units of 10^8cm/s, at a distance of 15 Kpc from the nucleus the mass flow $\dot{M}$, the kinetic energy density $\Phi(u_{ke})$, the energy density u_{ke} and the relativistic energy flow $\Phi(u_{eq})$ are respectively

$$\dot{M} \sim 0.1\, v_{fl} \qquad M_\odot/\text{year}$$

$$u_{ke} \sim 9\, 10^{-12} v_{fl,8}^2 \qquad \text{ergs/cm}^3$$

$$\sim 18\, u_{eq} \qquad \text{for a "free jet"}$$

$$\Phi(u_{ke}) \sim 4\, 10^{40} v_{fl,8}^3 \qquad \text{ergs/sec}$$

$$\sim 4\, 10^{42} \qquad \text{for a "free jet"}$$

$$\Phi(u_{eq}) \sim 3\, 10^{40} v_{fl,8} \qquad \text{ergs/sec}$$

The two energy flows $\Phi(u_{ke})$ and $\Phi(u_{eq})$ are comparable for $v_{fl,8} \sim 0.9$. So even for a moderately supersonic flow the kinetic energy term is dominant compared to the the relativistic one. Estimates on the energetics of the jet (or on $v_{fl,8}$) can be made by assuming that the broad components have been built by the energy transported by the jet in the lifetime of the source. From Table 7, we see that the energy stored in the broad components is

$$3\, 10^{56} < U_{br.c.} < 2\, 10^{57}$$

A lower limit to the source lifetime is clearly the time

$$\tau_d \sim (\text{jet length})/(\text{flow vel.}) \sim 7\, 10^7 (v_{fl,8})^{-1} \text{ years}$$

The average energy supply must therefore have been

$$< U_{br.c.}/\tau_d \sim (10^{41}-10^{42}) v_{fl,8} \quad \text{ergs/sec}$$

to be compared with $\Phi(u_{ke})$. This leads to:

$$v_{fl,8} < 2 - 6$$

So (unless the jet was much more powerful in the past) this argument also requires that its flow velocity should be in or below the range of values deduced from the "free jet" assumption.

We stress again that the discussion in Section 6a on the observed brightness-radius and depolarization-radius relations indicated that these could be explained if the mass flow increases and/or the velocity decreases along the jet. In this case, the kinetic energy flow must decrease along the jet and reconvert in some other form, either thermal or "useful energy" for synchrotron radiation. For the range of values of β discussed earlier, the decrease of $\Phi(_{ke})$ along the jet is very large, larger than that needed to compensate the adiabatic losses in the jet. One should therefore wonder where the lost energy goes. We suggest that it is used to feed the broad components, by some kind of leakage through the boundaries of the jet. We envisage a situation in which instabilities are produced at the boundaries of the jet and produce the growth of turbulence outside (e.g. Ferrari et al. 1978), in such a way that an energy outflow is produced at the expense of the reduction of the kinetic energy flow in the jet.

Finally it is worth commenting on the absence of hot spots at the end of the jets. The brightness at the end of the jets is comparable to that of the broad components in the eastern jet and only 2-3 times larger in the western one (see fig.2). Since it is generally assumed that the broad components are in pressure equilibrium with the static pressure of the external medium while the terminations of the jet should interact with it via ram-pressure, the ratio of the pressures in the jet and in the broad components ($\sim$3, derived from the brightness ratio via equipartition assumptions) gives the ratio of the "terminal velocity" to the external sound speed. The last velocity is likely to be $< 10^8$ cm/sec (for $T_e < 10^8$), so that the terminal velocity is likely to be $\gtrsim 1.5\, 10^8$ cm/sec. This figure compared with the above estimates of the flow velocity is a further argument for a decrease of the flow velocity along the jet.

c) Confinement of the jet at large distances

The slowly varying transverse size of the jet at distances > 2' may be considered an indication of confinement of the jet. Since the jet is completely embedded by the broad components, such a confinement, if external, must be produced by them. We have already seen that a reasonable estimate of the plasma density in the broad compnents is $\simeq 4\, 10^{-5}$ cm^{-3}. If the confinement is due to the static pressure of this thermal plasma, this requires:

$$T \sim 5\, 10^7 \text{ °K}$$

An alternative possibility (if the jet carries a net current) may be that the confinement is achieved by a pinch due to the circumferential field configuration $H_\perp$, as discussed by Bicknell and Henriksen (1980), Chan and Henriksen (1980), and Bridle et al.(1981).

These authors show that the magnetic field which would produce the observed change in the expansion rate by magnetic pinching in a cold jet (confinement) can be deduced from the relation

$$\frac{H^2}{4\pi\rho v_{fl}^2} = \varepsilon_\beta = \pi\gamma_m^2 / l_m$$

where γ_m is the maximum radius achieved and l_{max} is the distance from the core at which this γ_{max} is achieved. We find

$$\varepsilon_\beta \sim 0.014$$

which is consistent with our previous estimate of H and v_{fl}. The lack of any evident oscillations of the jet radius, according to the computations of the above authors, indicates that the ratio of magnetic to kinetic energy cannot be much larger than the above value (see for example the curves given for magnetized jets with both internal and external thermal pressures by Bridle et al.1981).

7. Conclusions

Summarizing, the most important results we have found are:

1) The source has an unusual morphology and can be described as a superimposition of a bright symmetric two sided jet on a double source.

2) The jet has a constant opening angle in the first 2' from the center; at larger distances the opening angle decreases and the transverse size seems stabilized.

3) The jet is strongly polarized at all frequencies; from the depolarization data we estimate the thermal plasma density in the range of 10^{-3} - 10^{-4} cm^{-3}.

4) The direction of the magnetic field is predominantly perpendicular to the jet axis.

5) The spectrum is flat and constant between 5GHz and 1.4GHz.

6) Over a significant fraction of the length of the jets, their brightness falls off more slowly with the jet radius than expected on the basis of adiabatic expansion in a constant velocity jet.

7) A constant mass flow along the jet, conservation of magnetic flux and constant flow velocity would together produce a variation of $H_{oz}\, n_i\, r$ different from that observed in our depolarization data. The behaviour of the brightness as well as of the depolarization could be explained if the flow velocity of the jet is decreasing as

$$v_{fl} \propto r^{-\beta} \quad \text{with} \quad 0.5 < \beta < 1.$$

It is suggested that most of the kinetic energy carried by the jet is flowing out of it across its boundary to form the extended radio structures surrounding the jet.

8) Several lines of argument suggest that typical flow velocities along the jet are less than, or of order, a few thousand km/sec.

Acknowledgments

We thank the staff of the WSRT and the reduction group for their work on the observations. We also thank Dr. Londrillo for several useful discussions and Dr. Zamorani for a critical reading of the manuscript and for many comments which greatly improved it.
We also thank L. Baldeschi and R. Primavera for preparing the figures and R. Kamer for help in revising the English and for typing the paper. This paper was prepared while one of us (R.F.) was visiting the Sterrewacht-Leiden. He gratefully acknowledges the hospitality and partial financial support.
The WSRT is operated by the Netherlands Foundation for Radio Astronomy with the financial support of the Netherlands Organization for the advancement of Pure Research (ZWO).
The National Radio Astronomy Observatory is operated by Associated Universities,Inc. under contract with the National Science Foundation.

References

Battistini, P., Bonoli, F., Silvestro, S., Fanti, R., Gioia, I.M., Giovannini, G.: 1980, Astron.Astrophys. 85,101.
Bridle, A.H., Chan, K.L., Henriksen, R.N.: 1981, J. Roy.Astron.Soc.can. 75, 69.
Bicknell, G.V., Henriksen, R.N.: 1980, Astrophys.Letters 21, 29.
Burn, B.J.: 1966, Mon.Not.Roy.Astr.Soc. 133, 67.
Chan, K.L., Henriksen, R.N.: 1980, Astrophys.J. 241, 534.
Colla, G., Fanti, C., Fanti, R., Gioia, I., Lari, C., Lequeux, J., Lucas, R., Ulrich, M.H.: 1975 , Astron. Astrophys.Suppl. 20, 1.
Ekers, R.D., Fanti, R., Lari, C., Parma, P.: 1981, Astron.Astrophys. 101, 194.
Ferrari, A., Trussoni, E., Zaninetti, L.: 1979, Astron. Astrophys. 79, 190.
Fomalont, E.B., Bridle, A.H., Willis, A.G., Perley, R.A.: . 1980, Astrophys.J. 237, 418.
Hargrave, P.J., McEllin, M.: 1975, Mon.Not.Roy.Astr.Soc. 173, 37.
Henriksen, R.N., Bridle, A.H., Chan, K.L.: 1982, Astrophys.J., in press.
Högbom,J.A., Brouw, W.N.: 1974, Astron.Astrophys. 33, 289.
Högbom, J.A.: 1974, Astron.Astrophys.Suppl. 15, 417.
Pacholczyk, A.G.: 1970, Radio Astrophysics, W.H. Freeman &Co.
Parma, P., Weiler, K.W.: 1981, Astron.Astrophys. 96, 412.
Perley, R.A., Willis, A.G., Scott, J.S.:1979, Nature 281, 437.
Tabara, H., Inoue, M.: 1980, Astron.Astrophys. 39, 379.
van Breugel, W.J.M., Willis, A.G.: 1981, Astron.Astrophys. 96, 332.
van Someren Grève, H.W.: 1974, Astron.Astrophys.Suppl. 15, 343.
Willis, A.G., Strom, R.G., Bridle, A.H., Fomalont, E.B.: 1981, Astron.Astrophys. 95, 250.

Errata added in proof

1. Line 20, l.h. column, p. 169 should read:
   ...explained if the flow velocity decreases and/or mass flow...
2. Line 40, l.h. column, p. 169 should read:
   The source, owing to its large angular size, was well...
3. In section (f) on p. 175 the 7 in the denominator of the r.h. side of the equation should be replaced by 5.